analytical chemistry

Article

pubs.acs.org/ac

Motor-Based Autonomous Microsensor for Motion and Counting Immunoassay of Cancer Biomarker

Xiaoping Yu, Yana Li, Jie Wu,* and Huangxian Ju

State Key Laboratory of Analytical Chemistry for Life Science, School of Chemistry and Chemical Engineering, Nanjing University, Nanjing 210093, P.R. China

Supporting Information

ABSTRACT: A motor-based autonomous microsensor is proposed for in situ visualization immunoassay of cancer biomarkers through motion readout or tag counting. The microsensor is prepared by functionalizing a newly designed gold-nanoparticle-modified self-propelled polyaniline/Pt (AuNP/PANI/Pt) micromotor with capture antibody. The autonomous movement of the microsensor in the fuel-enhanced sample mixture results in the fast and selective recognition of the protein target and subsequent loading of the secondary-antibody-modified glycidyl methacrylate microspheres (GMA), which slows down the movement of the sensing microengine. The velocity of the microsensor and the number of GMA conjugated on the microsensor can be conveniently visualized using optical microscopy. They are negatively and positively correlated with the target concentration, respectively. Therefore, the microsensor can conveniently distinguish the concentration of carcinoembryonic antigen in a range of 1−1000 ng/mL. The motor-based microsensor can be easily prepared in batch using AuNP/PANI/Pt. The whole detection procedure for protein target can be completed in 5 min without any washing and separation step. This method shows considerable promise for diverse clinical and diagnostic applications.

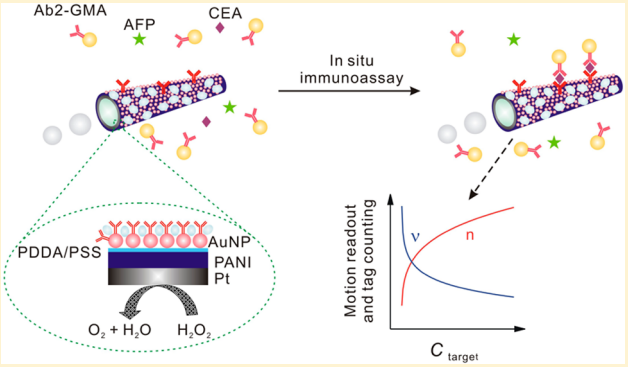

Immunosensors are miniaturized analytical devices that combine high selective biorecognition reactions with sensitive and convenient transducers. Compared with other immunoassay techniques, an immunosensor is cheaper, simpler, and more convenient.[1−3] Thus, various immunosensors including optical, mass-sensitive, and electrochemical immunosensors have been developed for the detection of cancer biomarkers, which are desired for effective cancer screening. However, their applications are facing great challenges because most of them require long assay time, multiple washing and separation steps, and diverse signaling reagents.

The emergence of nanotechnology has expanded the horizons of the immunosensor, as nanofabrication allows for miniaturization of the sensor, which improves the sensitivity and reduces the sample and reagent volumes, making the detection process more efficient.[4] In these sensing platforms, nanowires or nanotubes have been used as the transducers to label specific antibodies and construct miniaturized immunosensors.[5−8] By measuring the real-time conductivity change, the nanowire-based immunosensor enables label-free and high-throughput detection of cancer markers.[5] However, the nanosensors require sophisticated fabrication and detection instruments and professional operators, which greatly limit their application in resource-constrained communities or countries.

Here we report an attractive autonomous microsensor based on artificial micromotor for in situ, fast, and convenient visualization detection of cancer biomarkers. Inspired by the biomotors, which can autonomously move in aqueous solution and have the ability to capture and transport target proteins along microtubule tracks,[9,10] various artificial motors at nano/microscale have been designed on the basis of multitude of propulsion mechanisms.[11−21] Among these artificial motors, chemically powered catalytic tubular micromotors, whose movement has been driven by the decomposition of hydrogen peroxide, have been particularly attractive and powerful due to their efficient bubble-induced propulsion in relevant biological fluids and high-ionic-strength media, as desired for diverse practical applications.[22−24] Recently, Wang's group has reported a template-membrane-based synthesis to mass produce highly efficient polymer−metal bilayer micromotors.[25−27] Compared with pioneer rolled-up tubular micromotors,[28] such template-prepared tubular microbots display smaller size, faster propulsion speed, and lower cost. By functionalizing their surface with different bioreceptors, the bilayer micromotors have been used in recognition, transporting, and isolating of a wide array of target biomaterials in connection with the magnetic control and microchannel system.[29−31]

Received: January 28, 2014
Accepted: April 14, 2014
Published: April 14, 2014

   dx.doi.org/10.1021/ac500912c | *Anal. Chem.* 2014, 86, 4501−4507

The modification of specific bioreceptors on the micromotor is critical for its bioanalytical performance. Commonly, the biorecognition layer is constructed by sputtering the outer micromotor surface with a gold layer, followed by the self-assembly of the alkanethiol monolayer and covalent coupling of bioreceptors.[30,32−34] This procedure requires skilled e-beam deposition and can only modify half of the outer surface. Moreover, the velocity of the micromotors is also decreased by almost 75%,[30] which decreases the sensitivity of the micromotor. A recent report simplifies the modification procedure of copolymer/metal micromotor by coelectropolymerizing the functional monomer in the outer layer.[35] However, in order to maintain the morphology and performance of the micromotor, the active monomer should be doped with exact proportion, resulting in limited active sites on the surface of micromotor. Herein, a gold-nanoparticle-modified polyaniline/Pt (AuNP/PANI/Pt) micromotor and an autonomous microsensor were prepared through electrostatic assembly of AuNPs and then capture antibody (Ab1) on PANI/Pt (Scheme 1A). In the presence of target protein, the secondary-antibody-modified glycidyl methacrylate microspheres (Ab2-GMA) could quickly bind to the surface of the moving microsensor via the formation of a sandwich complex (Scheme 1B). The loading of microsize GMA tags on the microsensor slowed down its movement, resulting in a decrease of motion speed. Thus, a method for fast immunoassay of target protein was developed by motion readout or tag counting. Compared with the previous motor-based protein assays,[32,35] the proposed microsensor used AuNPs for surface modification, which increased the amount of capture antibody and thus showed highly efficient biosensing performance. In addition, the joint signal readout was proposed for sensing the immunoassay event, which greatly improved the detection sensitivity and accuracy. This was the first example of a motor-based microsensor for detection of cancer biomarker concentration. The microsensor possessed the advantages of easy fabrication, mass production, and low cost, showing great potential for diverse clinical and diagnostic applications.

Scheme 1. Schematic Illustration of (A) Motor-Based Microsensor Fabrication and (B) Use for in Situ Immunoassay of Protein Biomarker via Motion Readout and Tag Counting

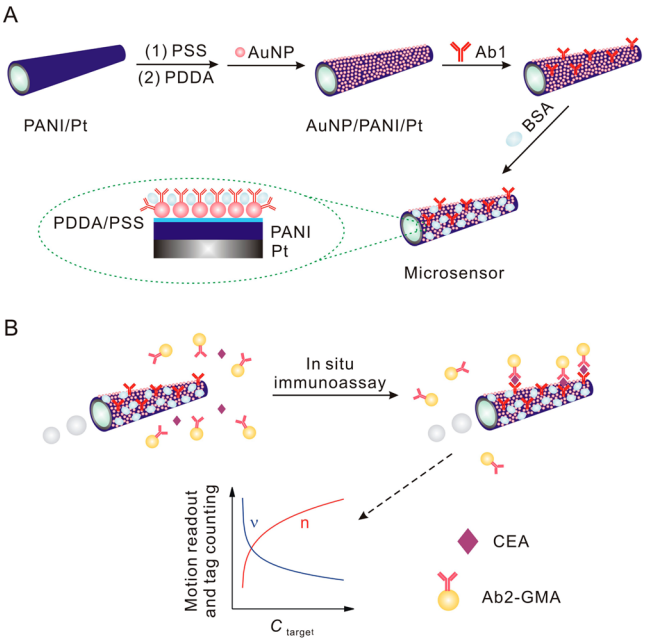

EXPERIMENTAL SECTION

Materials and Reagents. Aniline, dopamine hydrochloride (DA), and *o*-phenylenediamine (*o*-PD) were purchased from Alfa Aesar China Ltd. Sodium cholate hydrate (NaCh), fluoresceinamine, glutaraldehyde (GA), poly(diallyldimethylammonium chloride) (PDDA, MW ∼70 000), poly(sodium 4-styrenesulfonate) (PSS, MW ∼70 000, powder), 3,3′-dithiodipropionic acid di(*N*-hydroxysuccinimide ester) (DSP), and bovine serum albumin (BSA) were purchased from Sigma-Aldrich Chemical Co. (St. Louis, MO). Chloroplatinic acid ($HPtCl_6{\cdot}6H_2O$) was obtained from Shanghai Reagent Co. (Shanghai, China). The aqueous suspension of GMA coated with epoxy group (2.5% w/v, diameter 2 μm) was obtained from the Tianjin Baseline Chromtech Research Centre (China). Both Ab1 and Ab2 of anticarcinoembryonic antigen (CEA) (mouse monoclonal antibodies, clone no. bsm-1023 and bsm-1024) were supported by Beijing Biosynthesis Biotechnology Co. Ltd. (Beijing, China). CEA and α-fetoprotein (AFP) were purchased from Beijing Keybiotech Co., Ltd. (Beijing, China). The clinical serum samples were from Jiangsu Cancer Hospital (Nanjing). Phosphate-buffered saline (PBS, 0.01 M, pH 9.0) was used as coupling buffer for the immobilization of Ab1. Washing buffer was 0.01 M PBS (pH 7.4) spiked with 0.05% Tween-20. Blocking buffer, which was used to block the residual reactive sites on the Ab1-modified micromotor, was 0.01 M PBS (pH 7.4) containing 5% BSA. Other reagents were of analytical grade and used as received. Ultrapure water obtained from a Millipore water purification system (≥18 MΩ, Milli-Q, Millipore) was used in all assays.

Apparatus. Template electrochemical deposition of tubular micromotor was carried out with a CHI 660B electrochemical workstation (CH Instruments Inc., U.S.A.). The morphology of micromotor was examined using both scanning electron microscope (SEM) (Hitachi S-4800, Japan) and transmission electron microscope (TEM) (JEM-2100, JEOL, Japan). Images and videos were captured by Leica DMI 3000B inverted microscope equipped with a Photometrics Evolve 512/SC camera (Roper Scientific, Duluth, GA), and acquired at a frame rate of 10 frames/s using the Leica MM AF 1.5 software. Fluorescence images were captured by OLYMPUS IX71 microscope equipped with a CoolSNAP MYO camera.

Synthesis of Micromotor. The polymer−metal bilayer micromotors were prepared using a common template-directed electrodeposition protocol.[25,27] Briefly, a polycarbonate membrane, containing 2 μm diameter micropores (catalog no. TTTP02500; Millipore, Ireland), was employed as the template. A 75 nm gold film was first sputtered on one side of the porous membrane to serve as working electrode. A Pt wire and a saturated calomel electrode (SCE) were used as counter and reference electrodes, respectively. The membrane was then assembled in a plating cell with an aluminum foil serving as contact. PANI/Pt micromotors were prepared following sequential electrochemical plating of polymer and metal: the outer polymer layer was electropolymerized at +0.80 V for 0.06 C from the polymer plating solution containing 0.1 M H_2SO_4, 0.5 M Na_2SO_4, and 0.1 M freshly distilled aniline; the inner Pt layer was deposited galvanostatically at −2 mA for 1 h from a plating solution containing 18 mM H_2PtCl_6 and 0.05 M HCl. Subsequently, the sputtered gold film was completely

dx.doi.org/10.1021/ac500912c | Anal. Chem. 2014, 86, 4501−4507

removed by polishing with 1 μm alumina slurry. The membrane was then dissolved in methylene chloride for 15 min to release the micromotors, which were collected by centrifugation and washed repeatedly with methylene chloride, ethanol, and ultrapure water, respectively.

Similarly, DA and *o*-PD-doped PANI/Pt micromotors (PANI:DA/Pt and PANI:PD/Pt) were synthesized with a modified polymer plating process. The outer polymer layer of PANI:DA/Pt micromotor was synthesized by coelectropolymerization of aniline and DA up to 0.1 C at +0.4 V from the electroplating solution containing 0.1 M freshly distilled aniline, 0.1 M DA, 0.1 M H_2SO_4, and 0.5 M Na_2SO_4; and the polymer layer of PANI:PD/Pt was electropolymerized by cyclic voltammetry from −0.25 V to +0.8 V for 40 cycles in the mixture solution containing 0.05 M freshly distilled aniline, 0.05 M recrystallized *o*-PD, 0.4 M KCl, and 0.1 M HCl. Following the metal plating, polish movement, membrane dissolution, and washing steps analogous to the fabrication of PANI/Pt micromotors, both PANI:DA/Pt and PANI:PD/Pt micromotors were collected and stored in ultrapure water at room temperature before usage.

Fabrication of Microsensor. The fabrication of the motor-based microsensor was illustrated in Scheme 1A. The PANI/Pt micromotors were sequentially incubated with PSS and PDDA (0.1 mg/mL) for 30 min, respectively. The resulting micromotors underwent centrifugation with ultrapure water to remove excess polyelectrolyte. Then, citrate-wrapped AuNPs with 13 nm diameter[36] were added to the polyelectrolyte-functionalized micromotors under vigorous stirring for 1 h at room temperature. The unattached AuNPs were isolated by centrifugation (6000 rpm) with ultrapure water, and the obtained AuNP/PANI/Pt micromotor was dispersed in coupling buffer. Subsequently, Ab1 (33 μg/mL) was added into the AuNP/PANI/Pt suspension, followed by incubation at room temperature for 2 h with gentle shaking. Afterward, the micromotor was collected by centrifugation and dispersed in blocking buffer for 1 h to block the unmodified free surface of AuNPs. After washing by washing buffer, the motor-based microsensors were prepared and stored in PBS (10 mM, pH 7.4) at 4 °C before usage.

Fluorescent Measurement. The synthesized PANI/Pt, PANI:DA/Pt, and PANI:PD/Pt were incubated with 2.5% glutaraldehyde under shaking for 2 h, respectively, to obtain GA actived micromotors (GA-PANI/Pt, GA-PANI:DA/Pt, and GA-PANI:PD/Pt). Meanwhile, the AuNP/PANI/Pt micromotors were incubated with 5 mM DSP overnight to produce DSP-assembled AuNP/PANI/Pt (DSP-AuNP/PANI/Pt). After washing with water, all the functionalized micromotors including GA-PANI/Pt, GA-PANI:DA/Pt, GA-PANI:PD/Pt, and DSP-AuNP/PANI/Pt, as well as the bare PANI/Pt, were reacted with 100 μM fluoresceinamine aqueous solution overnight, respectively, to covalent bind fluoresceinamine on the outer surface of micromotors. All these fluoresceinamine-conjugated micromotors were washed and collected to capture fluorescence images.

Preparation of Ab2-GMA. Fifty microliters of the GMA suspension was washed with washing buffer three times and then resuspended in 100 μL of PBS (10 mM, pH 7.4) containing 33 μg/mL Ab2 for covalent linking under gentle stirring at room temperature for 45 min. Then, the Ab2-immobilized GMA microspheres were collected by centrifuge and blocked with blocking buffer for 1 h. After thoroughly washing with washing buffer, Ab2-GMA were dispensed in 100 μL of PBS (10 mM, pH 7.4) and kept at 4 °C before use.

Microsensor for Immunoassay of Protein Biomarker. The microsensor-based immunoassay of protein biomarkers was illustrated in Scheme 1B. Five microliters of microsensor, Ab2-GMA, 5% (w/v) NaCh, CEA standard solutions at different concentrations or serum samples, and 6% H_2O_2 solution were mixed, respectively, and dropped immediately on the glass slides for video acquisition and tracking. The final concentration of H_2O_2 was 1.2%. The movement of microsensor, the capture of Ab2-GMA, and the number of GMA on microsensor were visualized by the inverted optical microscope. The velocity of microsensor was calculated by tracking the object's center-to-center displacement from frame to frame.

RESULTS AND DISCUSSION

Characterization of AuNP/PANI/Pt. Typical SEM and TEM images showed a uniform and smooth morphology of the outer polymer layer of the template-synthesized PANI/Pt (Figure 1a,c). After the PANI/Pt micromotor was sequentially

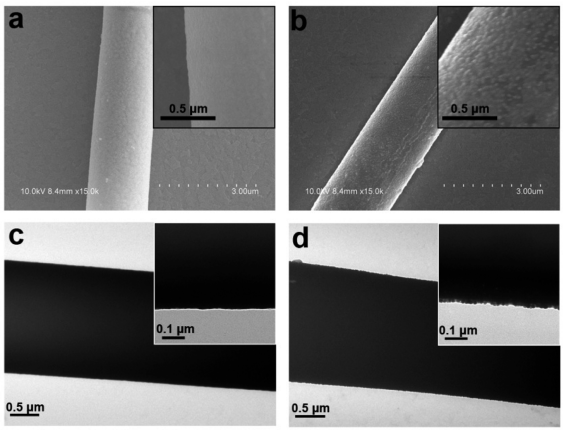

Figure 1. SEM (a, b) and TEM (c, d) images of (a, c) PANI/Pt and (b, d) AuNP/PANI/Pt micromotors. Inset: magnified pictures.

incubated with the oppositely charged PSS and PDDA polyelectrolytes, the outer surface of PANI/Pt was capped with positive charge, which facilitated the adsorption of the negatively charged citrate-wrapped AuNPs on PANI/Pt by electrostatic interactions. As shown in SEM (Figure 1b) and TEM (Figure 1d) images, numerous, individual "nanodots" were monolayer adsorbed on the surface of PANI/Pt, indicating the successful fabrication of AuNP/PANI/Pt.

Surface Modification of Micromotor. In order to obtain high efficient performance, the fabrication of microsensor, particularly the modification step of Ab1 on the micromotor surface, was concerned intensively. In this work, fluoresceinamine was used to mimic the amino-group of Ab1 and evaluate the functionalization of Ab1 on micromotors. As shown in Figure 2a,b, fluoresceinamine could not be modified on the outer polymer surface of PANI/Pt by neither direct absorption nor GA-based covalent bonding, suggesting few active sites, for example, bonding charge and free amino group, were available for the modification of Ab1. Compared with PANI/Pt microtube, slightly more fluoresceinamine was observed on both PANI:PD/Pt and PANI:DA/Pt (Figure 2c,d), indicating copolymerization of another monomer containing free active group[35] could not bring enough active sites on the outer

dx.doi.org/10.1021/ac500912c | *Anal. Chem.* 2014, 86, 4501−4507

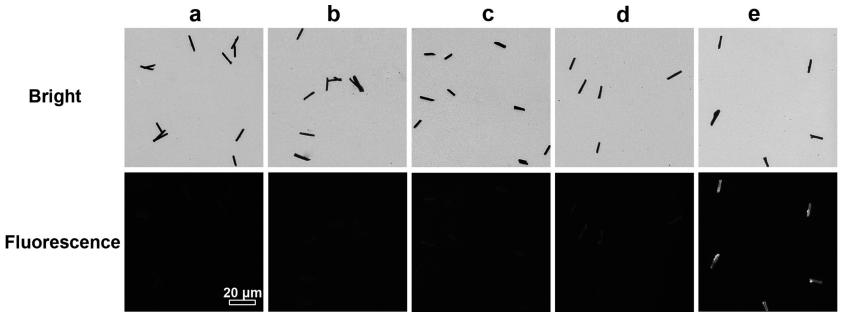

Figure 2. Fluorescence images of (a) bare PANI/Pt, (b) GA-PANI/Pt, (c) GA-PANI:PD/Pt, (d) GA-PANI:DA/Pt, and (e) DSP-AuNP/PANI/Pt micromotors incubated with 100 μM fluoresceinamine overnight. Scale bar = 20 μm.

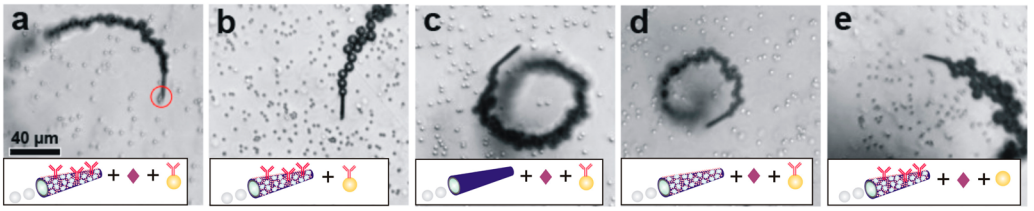

Figure 3. Time-lapse images of microsensor (a, b, e), bare PANI/Pt (c), and BSA-modified PANI/Pt (d) after navigation for 5 min in the fuel-filled solution containing (a, c, d) Ab2-GMA and 10 ng/mL CEA, (b) Ab2-GMA, and (e) free GMA and 10 ng/mL CEA. Scale bar = 40 μm.

polymer layer of the micromotor. However, strong fluorescence was well-distributed on the surface of AuNP/PANI/Pt (Figure 2e). This phenomenon was attributed to the uniform and density absorption of AuNPs on the outer polymer, which led to large surface area and more substantial active sites for fluoresceinamine conjugation. Thus, combined with the additional advantages of AuNPs of good biocompatibility and easy functionalization with protein, in the present work, AuNP/PANI/Pt was chosen for the immobilization of Ab1 and fabrication of microsensor.

The effects of the density and diameter of the AuNPs on the microsensor performance were also examined. With the increasing density of AuNPs on the outer surface, the number of GMA tag captured on the microsensor increased (Figure S1 in Supporting Information), which was attributed to the increase of captured antibody due to the increasing surface area. In addition, compared with the 13 nm AuNPs, 50 nm AuNPs could not be uniformly distributed on the outer surface of micromotor, thus making the detection accuracy worse (Figure S1 in Supporting Information). This work used 13 nm AuNPs with a relatively high density to fabricate the microsensor.

Microsensor for Immunoassay of Protein Marker. By modifying Ab1 on the AuNP/PANI/Pt micromotor, this work fabricated an autonomous microsensor for in situ immunoassay of cancer biomarkers. As shown in Figure 3 and Video S-1 in Supporting Information, the microsensor moved quickly through the fuel-filled detection solution and crashed into the stationary Ab2-GMAs frequently. In the presence of target protein, the microsensor could pick up Ab2-GMA quickly after their contact due to the sandwich immunoconjugation (Figure 3a). Furthermore, the movement of microsensor made its front end easier to contact the static Ab2-GMA. Hence in most cases, particularly in the solution containing a low level of target, Ab2-GMA bonded only on the outer surface near the front end of the microsensor, which was also observed in previous works.[30,34,35] The binding did not obviously affect the fuel supply.[25] The carriage of microsized GMA tag slowed the motion of microsensor. For example, in the presence of 10 ng/mL CEA, 5 GMA tags were observed on the microsensor surface along with a 26% decrease of the velocity of microsensor. In contrast, the GMA tag could not be captured by the microsensor in the absence of target even with many contacts, and the velocity of the microsensor was constant in a long navigation time (Figure 3b). Furthermore, no pickup events and changes of the velocity were observed in the control experiments using bare PANI/Pt micromotor (Figure 3c), BSA modified PANI/Pt micromotor (Figure 3d), or free GMA tags (Figure 3e). These results demonstrated that the microsensor could detect target protein specifically and was feasible to reflect the level of target protein in the sample by using both the motion and tag number.

Optimization of Assay Time. For real application, particularly for point-of-care testing, fast detection is one of the most important features of an immunosensor. In this work, the microsensor was added in the fuel and tag-filled sample solution to perform "on-the-fly" detection of protein biomarkers. Through the autonomous movement, the microsensor could recognize target protein and pick up Ab2-GMA rapidly.[33] As shown in Figure 4, the number of Ab2-GMA captured on

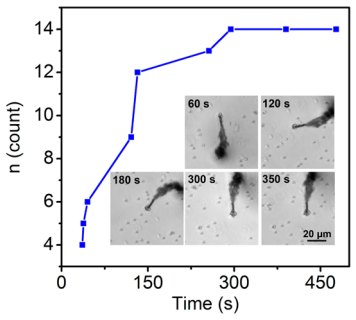

Figure 4. Effect of navigation time on the number of GMA tag captured on microsensor at 500 ng/mL CEA. Inset: time-lapse images taken after navigation for 60, 120, 180, 300, and 350 s. Scale bar = 20 μm.

dx.doi.org/10.1021/ac500912c | Anal. Chem. 2014, 86, 4501−4507

microsensor increased sharply with increasing incubation time and reached the saturation capacity after 5 min, indicating 5 min was enough for the protein detection by the proposed motor-based microsensor. Thus, 5 min was chosen for the immunoassay of protein. During the 5 min navigation, the normalized velocity (N_v) of the microsensor decreased only by 4% (Figure S2 in Supporting Information), indicating a negligible effect on the speed of the motor.

Assay Performance. The motion and tag responses of the microsensor after a 5 min movement in solutions containing different concentrations of CEA were represented in Figure 5

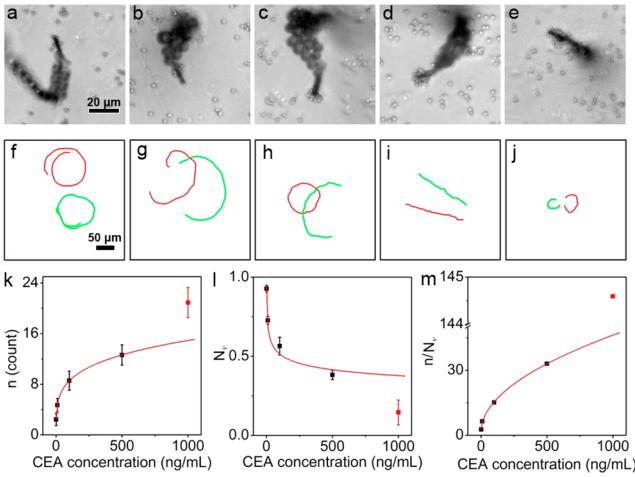

Figure 5. Time-lapse images (a–e) and track lines (f–j) of microsensor in the fuel filled solution containing Ab2-GMA and (a, f) 1, (b, g) 10, (c, h) 100, (d, i) 500, and (e, j) 1000 ng/mL CEA. Time-lapse images were taken after 5 min navigation and shown with a scale bar of 20 μm, and track lines were over a 3 s period and shown with a scale bar of 50 μm. (k–m) Dependence of captured GMA tag number (k), normalized microsensor velocity (l), and ratio of tag number to microsensor velocity (m) on CEA concentration. The error bars were estimated as the standard deviation of 15 microsensors.

and Video S-2 in Supporting Information. With the increasing CEA concentration, the number (n) of GMA tag conjugated on the microsensor increased (Figure 5a–e), whereas the velocity (v) as well as the track distance of the microsensor decreased (Figure 5f–j). Thus, based on the tag number and motion signal, each micromotor could be used as a microsensor to in situ reflect the concentration of protein biomarkers. Considering the difference of microsensor velocity among batches, the normalized velocity (N_v) was used for target detection. As shown in Figure 5, both the tag number (n) (Figure 5k) and normalized velocity response (N_v) (Figure 5l) showed low power exponential function relationships with the CEA concentration from 1 to 500 ng/mL. The regression equations were $n = 3.4\ C^{0.22} - 0.97$ and $N_v = 0.97\ C^{-0.13} - 0.028$, with the correlation coefficients of 0.999 and 0.974, respectively. Although the exponential value of the counting readout was 1.7 times higher than that of motion readout (0.22 vs. 0.13), they were much lower than 1, suggesting the microsensor was suitable for semiquantitative rather than precise analysis of CEA at low level by using individual signal of counting and motion. However, as the tag number and motion signal were positively and negatively correlated, respectively, with the target concentration, the detection sensitivity and accuracy of microsensor could be improved greatly by using the joint signal readout of n/N_v (Figure 5m). The regression equation of n/N_v and CEA concentration was $n/N_v = 1.34\ C^{0.51} + 1.60$, showing 2.3 and 3.9 times higher exponential change than that using individual tag number and motion readout, respectively. The wide detection range, along with the convenient diverse signal readout, made the proposed motor-based microsensor a valuable candidate of traditional ELISA, showing considerable promise in point-of-care detection.

Selectivity and Reproducibility of Microsensor. The specificity of the micromotor-based sensing protocol was evaluated by challenging the microsensor toward different protein markers. Figure 6 and the corresponding Video S-3 in Supporting Information illustrated the microsensor after a 5 min movement in solutions containing either CEA or other antigen only, for example, AFP, and the mixture of CEA and AFP. As expected, obvious capture of the GMA tag on the microsensor was only observed in the solution containing target CEA (Figure 6c,d), whereas no binding event was observed in AFP solution (Figure 6b), indicating high detection specificity of the proposed microsensor.

The reproducibility of microsensor was investigated by using 3 different batches of the microsensors to detect 500 ng/mL CEA. All the microsensors were able to recognize and capture Ab2-GMA tags efficiently. The coefficients of variation (RSD) of both tag number and motion response were 12.7% and 7.8%, respectively, indicating acceptable precision and fabrication reproducibility.

Real Sample Analysis. To evaluate the analytical reliability and application potential, the proposed microsensor was used for semiquantitative analysis of CEA in the untreated serum samples. Although the original velocity of microsensor in serum was 88.68 μm/s, which was lower than that of 140.24 μm/s in buffer solution due to the higher viscosity of serum sample, the normalized velocity (N_v) as well as the tag number used for target detection eliminated the effect of original velocity divergence. In addition, the effect of H_2O_2 degradation was also negligible during 5 min detection time (Figure S3 in Supporting Information). As shown in Figure 7 and the

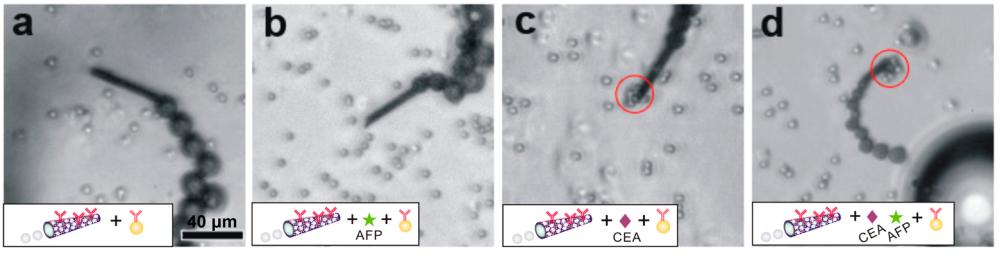

Figure 6. Time-lapse images of microsensor after navigation for 5 min in fuel and Ab2-GMA-filled solution (a), (a) + 10 ng/mL AFP (b), (a) + 10 ng/mL CEA (c), and (a) + 10 ng/mL CEA + 10 ng/mL AFP (d). Scale bar = 20 μm.

dx.doi.org/10.1021/ac500912c | Anal. Chem. 2014, 86, 4501–4507

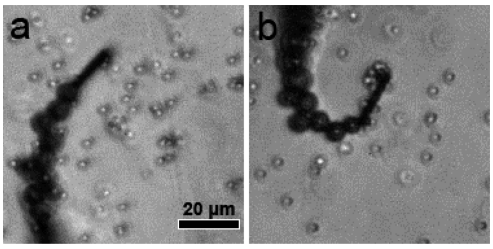

Figure 7. Time-lapse images of microsensor after navigation for 5 min in fuel and Ab2-GMA-filled serum samples from patients. Scale bar = 20 μm.

corresponding Video S-4 in Supporting Information, 2 and 10 GMA microspheres, along with the normalized velocities of 0.765 and 0.508, were observed on microsensor in sample 1 and sample 2, respectively. Thus, the CEA concentrations in sample 1 and sample 2 were detected to be at levels of 1−10 and 100−500 ng/mL, respectively, which were in agreement with those (5.2 ng/mL for sample 1 and 102.5 ng/mL for sample 2) from the commercial electrochemiluminescent testing, suggesting good accuracy of the proposed microsensor for the detection of clinical samples.

CONCLUSIONS

This work proposes a motor-based autonomous microsensor for in situ, fast, and convenient detection of cancer biomarkers. The microsensor is fabricated on a gold-nanoparticle-modified self-propelled PANI/Pt micromotor. The AuNPs offer plentiful active sites and good biocompatibility to Ab1 for facilitating the sensor fabrication and improving the sensing performance. The autonomous movement of the microsensor accelerates the sandwich immunoreactions, thus the immunoassay can be carried out within 5 min without any washing and separation step. In addition, by using the motion readout and tag counting, the microsensor can conveniently reflect the level of the target protein with the visualization technique. This concept can be expanded to quantify other proteins and nucleic acid markers. Benefitting from the easy fabrication, mass production, low cost, and simple operation and detection, the proposed microsensor shows great potential for point-of-care testing and early cancer screening, especially in resource-constrained communities or countries.

ASSOCIATED CONTENT

Supporting Information

Additional information as noted in the text. This material is available free of charge via the Internet at http://pubs.acs.org.

AUTHOR INFORMATION

Corresponding Author

*E-mail: wujie@nju.edu.cn. Tel./Fax: +86-25-83593593.

Notes

The authors declare no competing financial interest.

ACKNOWLEDGMENTS

We gratefully acknowledge the National Basic Research Program (2010CB732400), National Natural Science Foundation of China (21105046, 21135002, and 21121091), PhD Fund for Young Teachers (20110091120012), and Natural Science Foundation of Jiangsu (BK2011552).

REFERENCES

(1) Wang, J. *Biosens. Bioelectron.* **2006**, *21*, 1887−1892.
(2) Wu, J.; Fu, Z. F.; Yan, F.; Ju, H. X. *TrAC, Trends Anal. Chem.* **2007**, *26*, 679−688.
(3) Sergey, M. B.; Wolfbeis, O. S. *Chem. Rev.* **2008**, *108*, 423−461.
(4) Jain, K. K. *Clin. Chim. Acta* **2005**, *358*, 37−54.
(5) Zheng, G. F.; Patolsky, F.; Cui, Y.; Wang, W. U.; Lieber, C. M. *Nat. Biotechnol.* **2005**, *23*, 1294−1301.
(6) Cui, Y.; Wei, Q. Q.; Park, H. K.; Lieber, C. M. *Science* **2001**, *293*, 1289−1292.
(7) Wohlstadter, J. N.; Wilbur, J. L.; Sigal, G. B.; Biebuyck, H. A.; Billadeau, M. A.; Dong, L. W.; Fischer, A. B.; Gudibande, S. R.; Jamieson, S. H.; Kenten, J. H.; Leginus, J.; Leland, J. K.; Massey, R. J.; Wohlstadter, S. J. *Adv. Mater.* **2003**, *15*, 1184−1187.
(8) Patolsky, F.; Zheng, G. F.; Hayden, O.; Lakadamyali, M.; Zhuang, X. W.; Lieber, C. M. *Proc. Natl. Acad. Sci. U.S.A.* **2004**, *101*, 14017−14022.
(9) Lin, C. T.; Kao, M. T.; Kurabayashi, K.; Meyhofer, E. *Nano Lett.* **2008**, *8*, 1041−1046.
(10) Fischer, T.; Agarwal, A.; Hess, H. *Nat. Nanotechnol.* **2009**, *4*, 162−166.
(11) Paxton, W. F.; Baker, P. T.; Kline, T. R.; Wang, Y.; Mallouk, T. E.; Sen, A. *J. Am. Chem. Soc.* **2006**, *128*, 14881−14888.
(12) Gao, W.; Sattayasamitsathit, S.; Manesh, K. M.; Weihs, D.; Wang, J. *J. Am. Chem. Soc.* **2010**, *132*, 14403−14405.
(13) Gao, W.; Pei, A.; Wang, J. *ACS Nano* **2012**, *6*, 8432−8438.
(14) Mou, F. Z.; Chen, C. R.; Ma, H. R.; Yin, Y. X.; Wu, Q. Z.; Guan, J. G. *Angew. Chem., Int. Ed.* **2013**, *52*, 1−6.
(15) Wilson, D. A.; Nolte, R. J. M.; van Hest, J. C. M. *Nat. Chem.* **2012**, *4*, 268−274.
(16) Wu, Z. G.; Wu, Y. J.; He, W. P.; Lin, X. K.; Sun, J. M.; He, Q. *Angew. Chem., Int. Ed.* **2013**, *52*, 7000−7003.
(17) Dong, B.; Zhou, T.; Zhang, H.; Li, C. Y. *ACS Nano* **2013**, *7*, 5192−5198.
(18) Garcia-Gradilla, X.; Orozco, J.; Sattayasamitsathit, S.; Soto, F.; Kuralay, F.; Pourazary, A.; Katzenberg, A.; Gao, W.; Shen, Y. F.; Wang, J. *ACS Nano* **2013**, *7*, 9232−9240.
(19) Paxton, W. F.; Sundararajan, S.; Mallouk, T. E.; Sen, A. *Angew. Chem., Int. Ed.* **2006**, *45*, 5420−5429.
(20) Gao, W.; Sattayasamitsathit, S.; Wang, J. *Chem. Rec.* **2012**, *12*, 224−231.
(21) Mei, Y. F.; Solovev, A. A.; Sanchez, S.; Schmidt, O. G. *Chem. Soc. Rev.* **2011**, *40*, 2109−2119.
(22) Solovev, A. A.; Mei, Y. F.; Urena, E. B.; Huang, G. S.; Schmidt, O. G. *Small* **2009**, *5*, 1688−1692.
(23) Sanchez, S.; Solovev, A. A.; Mei, Y. F.; Schmidt, O. G. *J. Am. Chem. Soc.* **2010**, *132*, 13144−13145.
(24) Manesh, K. M.; Cardona, M.; Yuan, R.; Clark, M.; Kagan, D.; Balasubramanian, S.; Wang, J. *ACS Nano* **2010**, *4*, 1799−1804.
(25) Gao, W.; Sattayasamitsathit, S.; Orozco, J.; Wang, J. *J. Am. Chem. Soc.* **2011**, *133*, 11862−11864.
(26) Gao, W.; Uygun, A.; Wang, J. *J. Am. Chem. Soc.* **2012**, *134*, 897−900.
(27) Gao, W.; Sattayasamitsathit, S.; Uygun, A.; Pei, A.; Ponedal, A.; Wang, J. *Nanoscale* **2012**, *4*, 2447−2453.
(28) Solovev, A. A.; Sanchez, S.; Pumera, M.; Mei, Y. F.; Schmidt, O. G. *Adv. Funct. Mater.* **2010**, *20*, 2430−2435.
(29) Orozco, J.; Cortés, A.; Cheng, G. Z.; Sattayasamitsathit, S.; Gao, W.; Feng, X. M.; Shen, Y. F.; Wang, J. *J. Am. Chem. Soc.* **2013**, *135*, 5336−5339.
(30) Campuzano, S.; Orozoc, J.; Kagan, D.; Guix, M.; Gao, W.; Sattayasamitsathit, S.; Claussen, J. C.; Merkoci, A.; Wang, J. *Nano Lett.* **2012**, *12*, 396−401.
(31) Wang, Y.; Fei, S.; Byun, Y. M.; Lammert, P. E.; Crespi, V. H.; Sen, A. *J. Am. Chem. Soc.* **2009**, *131*, 9926−9927.
(32) Orozco, J.; Campuzano, S.; Kagan, D.; Zhou, M.; Gao, W.; Wang, J. *Anal. Chem.* **2011**, *83*, 7962−7969.
(33) Kagan, D.; Campuzano, S.; Balasubramanian, S.; Kuralay, F.; Flechsig, G. U.; Wang, J. *Nano Lett.* **2011**, *11*, 2083−2087.

(34) Balasubramanian, S.; Kagan, D.; Hu, C. M. J.; Campuzano, S.; Lobo-Castanon, M. J.; Lim, N.; Kang, D. Y.; Zimmerman, M.; Zhang, L. F.; Wang, J. *Angew. Chem., Int. Ed.* **2011**, *50*, 4161−4164.
(35) García, M.; Orozco, J.; Guix, M.; Gao, W.; Sattayasamitsathit, S.; Escarpa, A.; Merkoci, A.; Wang, J. *Nanoscale* **2013**, *5*, 1325−1331.
(36) Ambrosi, A.; Castaneda, M. T.; Killard, A. J.; Smyth, M. R.; Alegret, S.; Merkoci, A. *Anal. Chem.* **2007**, *79*, 5232−5240.